Dyes and Pigments 161 (2019) 382–388

Contents lists available at ScienceDirect

Dyes and Pigments

journal homepage: www.elsevier.com/locate/dyepig

An unconventional helical push-pull system for solar cells

Davide Dova[a], Silvia Cauteruccio[a,*,1], Norberto Manfredi[b,**,1], Stefan Prager[c], Andreas Dreuw[c], Serena Arnaboldi[a], Patrizia R. Mussini[a], Emanuela Licandro[a], Alessandro Abbotto[b]

[a] Dipartimento di Chimica, Università degli Studi di Milano, via Golgi 19, I-20133, Milan, Italy
[b] Department of Materials Science and Solar Energy Research Center MIB- SOLAR, University of Milano-Bicocca, and INSTM Milano-Bicocca Research Unit, Via Cozzi 55, I-20125, Milano, Italy
[c] Interdisciplinary Center for Scientific Computing, Heidelberg University, Im Neuenheimer Feld 368, 69120, Heidelberg, Germany

ARTICLE INFO

Keywords:
Push-pull chiral system
Tetrathiahelicene
Dye-sensitized solar cells

ABSTRACT

The synthesis, photophysical and electrochemical characterization, theoretical calculations and photovoltaic studies of a push-pull dye with an unconventional nonplanar tetrathiahelicene π−spacer between the donor-acceptor groups, are reported. The molecule exhibits suitable HOMO LUMO levels to be used in DSSC. The presence of the donor-acceptor helical architecture allows the internal charge transfer and subsequent electron injection to the conduction band of TiO_2 leading to the good photocurrent value of 4.6 mA cm^{-2}.

1. Introduction

Tetrathiahelicenes (7-THs), formed by thiophene and benzene rings *ortho*-fused in an alternating fashion, belong to an intriguing class of chiral helical-shaped molecules, that have reached a high degree of appeal thanks to the association of synthetic challenges to manifold applications in different areas of science [1]. The configurationally fixed helical arrangement confers them a peculiar topology and chirality, and has a strong impact on the electronic structure of the π-conjugated system, thus providing unique electronic and optical properties suitable for applications in optoelectronics [2], biomolecular recognition [3], and asymmetric catalysis [4]. The regioselective functionalization of the α-position(s) of the terminal thiophene ring(s) allows the introduction of a variety of substituents [5], which can further modulate specific properties, including electronic properties. At the same time the helical system can exhibit even a high degree of flexibility depending on the nature and dimension of substituents present on the terminal aryl rings [6]. In light of these considerations it is therefore quite surprising that the 7-TH has never been used as a π-linker in push-pull dyes for applications in dye-sensitized solar cells (DSSCs). In this paper we describe the first example of a push-pull dye in which the 7-TH scaffold has been used as the π-spacer between a donor and an acceptor group, and we investigate the photophysical and electrochemical properties. In addition, we also performed theoretical calculations and photovoltaic (PV) studies to assess their performance as helical-based push-pull dye.

We designed the novel helical dye system **1** (Fig. 1), that could fulfil the requirements as an organic donor-π-acceptor DSSC sensitizer, being constituted by: *i)* the thiahelicene scaffold as stable and π-conjugated-bridge spacer; *ii)* the triarylamine moiety connected to the heteroaromatic spacer by a vinylene linkage as a donor group; *iii)* the cyanoacrylic acid moiety as an electron acceptor and anchoring group for the covalent grafting to the TiO_2 surface. Two *n*-propyl chains are incorporated into the dye **1** to improve solubility and alleviate aggregation. As this regard, the non-planarity of the helical system along with the presence of the bulky triarylamine group should also disturb possible adverse π-stacking events, suppressing the aggregation of the dye molecules on the TiO_2 surface.

2. Experimental section

2.1. General methods

All commercially available reagents and solvents were used without further purification unless otherwise noted. Tetrathia[7]helicene-based aldehydes **2** and **6** were prepared according to literature [5d]. The phosphonium salt **3** was prepared as previously reported [7]. Thin-layer chromatography (TLC) was performed with Aldrich silica gel 60 F254 precoated plates, and plates were visualized with short-wave UV light (254 and 366 nm). Column chromatography was carried out with

* Corresponding author.
** Corresponding author.
E-mail addresses: silvia.cauteruccio@unimi.it (S. Cauteruccio), norberto.manfredi@unimib.it (N. Manfredi).
[1] These two authors contributed equally to the work.

https://doi.org/10.1016/j.dyepig.2018.09.050
Received 25 May 2018; Received in revised form 7 September 2018; Accepted 19 September 2018
Available online 26 September 2018
0143-7208/

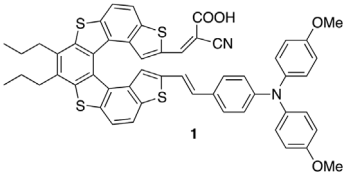

Fig. 1. Structure of dye **1**.

Aldrich silica gel (70–230 mesh). The ^{1}H and ^{13}C NMR spectra were recorded at 25 °C using Bruker AC-300 MHz, Bruker Avance III 400 MHz, Bruker AMX-500 MHz and Bruker Avance 600 MHz spectrometers. Chemical shifts (δ) were reported in parts per million calibrated against the residual protonated solvent resonances (^{1}H: δ = 2.05 ppm, ^{13}C: δ = 29.92 ppm for $(CD_3)_2CO$; ^{1}H: δ = 2.50 ppm, ^{13}C: δ = 39.51 ppm for DMSO-d_6). High-resolution mass spectra (HRMS) were recorded using a Bruker Daltonics ICR-FTMS (Fourier transform ion cyclotron resonance mass spectrometry) *APEX II*. The elemental analyses were recorded with a Perkin-Elmer 2400.

2.2. Syntheses

2.2.1. Synthesis of intermediate 4

A solution of **3** (120 mg, 0.18 mmol) in DMF (4 mL) was slowly added, under stirring at room temperature, to a suspension of **2** (117 mg, 0.21 mmol), K_2CO_3 (50 mg, 2.1 mmol), 18-crown-6 ether (9.5 mg, 0.036 mmol) in DMF (4 mL). The resulting reaction mixture was stirred at room temperature for 16 h. The mixture was then poured into water (10 mL), and the aqueous phase was extracted with CH_2Cl_2 (4 × 15 mL). The resulting organic layer was washed with water (2 × 10 mL), dried over anhydrous sodium sulphate, and filtered. The filtrate was evaporated, and the residue was purified by silica gel column chromatography using hexane and AcOEt (9:1 v/v) as eluent to give compound **4** (95 mg, 67%) as an orange solid. ^{1}H NMR (400 MHz, $(CD_3)_2SO$): δ 9.36 (s, 1H), 8.47 (d, 1H, J = 8.6 Hz), 8.39 (d, 1H, J = 8.8 Hz), 8.18 (s, 2H), 7.43 (s, 1H), 7.22 (d, 2H, J = 8.8 Hz), 7.05 (m, 4H), 6.94 (m, 4H), 6.68 (d, 2H, J = 8.7 Hz), 6.62 (d, 1H, J = 16 Hz), 6.47 (s, 1H), 6.43 (d, 1H, J = 16 Hz), 3.76 (s, 6H), 3.16 (m, 4H), 1.84 (m, 4H), 1.14 (t, 6H, J = 7.2 Hz). ^{13}C NMR (150 MHz, $(CD_3)_2CO$): δ 185.1 (CHO), 157.7 (C_q, 2C), 150.1 (C_q), 143.7 (C_q), 142.1 (C_q), 141.4 (C_q), 141.3 (C_q), 141.0 (C_q), 140.98 (C_q), 137.8 (C_q), 137.5 (C_q), 136.9 (C_q), 136.7 (C_q), 136.4 (CH), 135.9 (C_q), 134.2 (C_q, 2C), 133.6 (C_q), 133.3 (C_q), 131.7 (CH), 131.1 (C_q), 130.6 (CH), 129.2 (C_q), 129.1 (C_q), 128.53 (CH), 128.49 (C_q), 128.2 (CH, 4C), 128.0 (CH), 124.2 (CH), 124.0 (CH), 122.6 (CH), 122.2 (CH), 120.4 (CH), 119.8 (CH), 119.3 (CH), 115.9 (CH, 3C), 115.8 (CH), 56.0 (-OCH_3, 2C), 35.2 (CH_2, 2C), 24.3 (CH_2, 2C), 15.1 (CH_3, 2C). HRMS (ESI, positive mode) m/z: $[M]^+$ calcd for $C_{51}H_{41}NO_3S_4$ 843.1969, found 843.2075.

2.2.2. Synthesis of dye 1

Cyanoacetic acid (18.0 mg, 0.21 mmol) and piperidine (2 mg, 0.5 mmol) were added to a solution of **4** (41 mg, 0.05 mmol) in a mixture of THF (1 mL) and CH_3CN (10 mL) at room temperature. The resulting mixture was then stirred at reflux for 5 h. The solvents were removed under reduced pressure. The residue was taken up with an aqueous solution of HCl (0.1 M, 6 mL), the solid was filtered and washed with hexane and CH_3CN, and dried under vacuum to afford **1** (27 mg, 60%) as a red solid. ^{1}H NMR (600 MHz, $(CD_3)_2SO$): δ 8.39 (m, 2H), 8.14 (m, 2H), 7.72 (s, 1H), 7.32 (s, 1H), 7.22 (d, 2H, J = 8.6 Hz), 7.05 (d, 4H, J = 8.8 Hz), 6.93 (d, 4H, J = 8.8 Hz), 6.67 (d, 2H, J = 8.5 Hz), 6.63 (d, 1H, J = 16 Hz), 6.45 (s, 1H), 6.43 (d, 1H, J = 16 Hz), 3.75 (s, 6H), 3.12 (m, 4H), 1.82 (m, 4H), 1.13 (m, 6H). ^{13}C NMR (75 MHz, $(CD_3)_2CO$): δ 163.9 (C_q), 157.5 (C_q, 2C), 154.5 (CH), 149.9 (C_q), 147.2 (CH), 143.3 (C_q), 141.4 (C_q), 141.2 (C_q, 2C), 141.1 (C_q), 140.8 (C_q), 137.7 (C_q), 137.5 (CH), 137.4 (C_q), 136.7 (C_q), 136.6 (C_q), 135.2 (C_q), 134.7 (C_q), 134.1 (CH), 134.0 (C_q), 133.3 (C_q), 132.4 (C_q), 131.5 (CH), 130.9 (C_q), 129.4 (CH), 129.2 (C_q), 128.9 (C_q), 128.4 (CH), 128.0 (CH, 4C), 124.0 (CH), 123.7 (CH), 122.9 (C_q), 121.9 (CH), 120.3 (CH), 119.7 (CH), 119.2 (CH), 117.1 (CH), 116.5 (C_q), 116.1 (CH), 115.8 (CH, 2C), 102.9 (C_q), 55.8 (-OCH_3, 2C), 35.0 (CH_2, 2C), 24.1 (CH_2, 2C), 15.0 (CH_3, 2C). HRMS (ESI, positive mode) m/z: $[M]^+$ calcd for $C_{54}H_{42}N_2O_4S_4$ 910.2027, found 910.2064. Elemental anal. Found: C, 71.68; H, 4.38; N, 2.74%; molecular formula $C_{54}H_{42}N_2O_4S_4$ requires C, 71.18; H, 4.65; N, 3.07%. UV–vis (DCM), λ_{max} [ε (10^4 L mol^{-1} cm^{-1})]: 424 [5.14] nm.

2.2.3. Synthesis of dye 5

Cyanoacetic acid (48 mg, 0.58 mmol) and piperidine (4 mg, 0.046 mmol) were added to a solution of **6** (60 mg, 0.116 mmol) in THF (6 mL) at room temperature. The resulting mixture was then stirred at reflux for 5 h. The solvent was removed under reduced pressure. The residue was taken up with CH_2Cl_2 and an aqueous solution of HCl (0.2 M). The aqueous phase was extracted with CH_2Cl_2, and the resulting organic layer was washed with water, dried over anhydrous sodium sulphate, and filtered. The filtrate was evaporated, and the residue was purified by silica gel column chromatography using CH_2Cl_2 and MeOH (9:1 v/v) as eluent to give compound **5** (55 mg, 82%) as an orange solid. ^{1}H NMR (500 MHz, DMSO-d_6): δ 8.19–8.07 (m, 4H), 7.28 (s, 1H), 7.19 (d, 1H, J = 5.5 Hz), 6.86 (s, 1H), 6.41 (d, 1H, J = 5.5 Hz), 3.01 (m, 2H), 2.90 (m, 2H), 1.67 (m, 4H), 1.01–0.98 (m, 6H). ^{13}C NMR (125 MHz, DMSO-d_6): δ 163.1 (C_q), 140.5 (CH), 139.4 (C_q), 139.2 (C_q), 138.2 (C_q), 136.3 (C_q), 136.0 (C_q), 135.6 (C_q), 135.1 (C_q), 134.9 (C_q), 134.0 (C_q), 132.4 (C_q), 132.0 (CH), 131.9 (C_q), 130.5 (C_q), 130.1 (C_q), 127.3 (C_q), 127.0 (C_q), 125.8 (CH), 124.0 (CH), 121.7 (CH), 121.6 (CH), 121.3 (CH), 119.0 (CH), 118.2 (C_q), 111.0 (C_q), 33.6 (CH_2, 2C), 23.8 (CH_2, 2C), 14.4 (CH_3, 2C). MS (EI) m/z: 537 $[M-CO_2]^+$. HRMS (ESI, positive mode) m/z: $[M-CO_2]^+$ calcd for $C_{31}H_{23}NS_4$ 537.0713, found 537.0405. Elemental anal. Found: C, 66.23; H, 4.27; N, 2.30%; molecular formula $C_{32}H_{23}NO_2S_4$ requires C, 66.06; H, 3.98; N, 2.41%. UV–vis (DCM), λ_{max} [ε (10^4 L mol^{-1} cm^{-1})]: 434 [2.3] nm.

2.3. Optical and electrochemical measurements

UV–vis spectra of compounds **1** and **5** were recorded with a V-570 Jasco spectrophotometer.

Cyclic voltammetry (CV) studies were performed at potential scan rates typically ranging 0.05–2 V s^{-1} in CH_2Cl_2 solutions 0.0005 M and 0.00075 M, deaerated by N_2 bubbling, with tetrabutylammonium perchlorate TBAP 0.1 M as the supporting electrolyte, at 298 K. The ohmic drop has been compensated by the positive feedback technique. The experiments were carried out using an AUTOLAB PGSTAT potentiostat (EcoChemie, The Netherlands) run by a PC with GPES software. The working electrode was a glassy carbon (GC) one (AMEL, diameter = 1.5 mm) cleaned by diamond powder (Aldrich, diameter = 1 μm) on a wet cloth (STRUERS DP-NAP); the counter electrode was a platinum wire; the reference electrode was an aqueous saturated calomel electrode (SCE), having in our working solvent (CH_2Cl_2) a difference of −0.495 V *vs.* the $Fc^+|Fc$ couple (the inter-solvental redox potential reference currently recommended by IUPAC) and inserted in a double bridge in order to prevent water and/or chloride leakage. The HOMO and LUMO values were estimated with the formula: HOMO (LUMO) = − e [E_p, I_a *vs* $Fc^+|Fc$ (E_p, I_c *vs* $Fc^+|Fc$) + 4.8], where e is the unitary charge, E_p, I_a and E_p, I_c are the first oxidation and reduction peaks, respectively and +4.8 is the recommended value to be consistent with the absolute value for the normal hydrogen electrode.

2.4. Computational studies

The equilibrium geometry of **1** has been optimized using density functional theory (DFT) employing the ωB97XD [8] exchange-correlation functional in combination with the cc-pVDZ basis set [9]. The

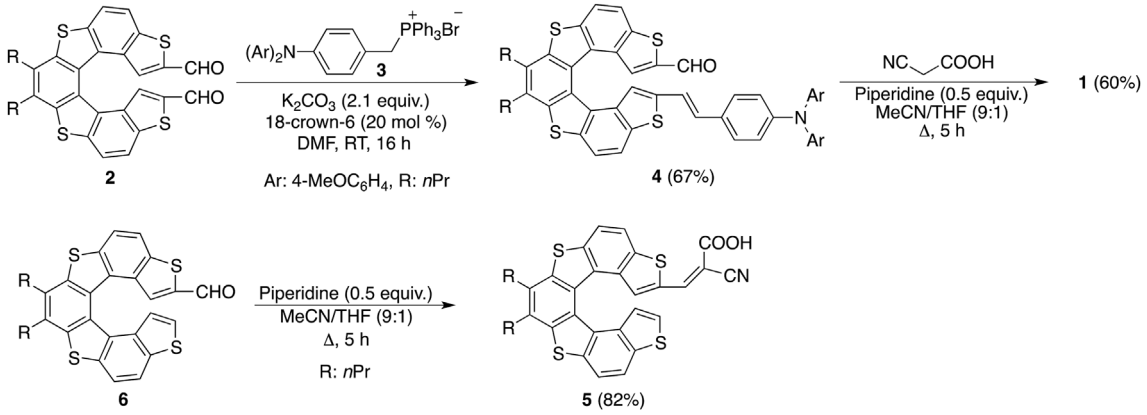

Scheme 1. Synthesis of dyes **1** and **5**.

optical properties of **1** have been investigated theoretically using time-dependent density functional theory (TD-DFT) employing the same functional and basis set as used for the ground state calculations. For all calculations, the Gaussian 09 Rev. D.01 [10] program package was used. Orbitals and molecular structures were visualized using Avogadro 1.1.0 [11] and rendered using PovRay 3.7.0 [12].

2.5. Photovoltaic measurements

The following materials were purchased from commercial suppliers: FTO-coated glass plates (2.2 mm thick; sheet resistance ~7 Ω/square; Solaronix); TiO_2 (Solaronix T/SP and R/SP); N719 (Sigma-Aldrich). The thickness of the layers was measured by means of a VEECO Dektak 8 Stylus Profiler. Photovoltaic measurements of DSSCs were carried out with an antireflective layer and with or without black mask on top of the photoanode of 0.38 cm^2 surface area under a 500 W Xenon light source. The power of the simulated light was calibrated to AM 1.5 (100 mW cm^{-2}) using a reference Si cell photodiode equipped with an IR-cutoff filter (KG-5) to reduce the mismatch in the region of 350–750 nm between the simulated light and the AM 1.5 spectrum. Values were recorded after 3 and 24 h, 3 and 6 days of ageing in the dark. I–V curves were obtained by applying an external bias to the cell and measuring the generated photocurrent with a Keithley digital source meter. IPCE were recorded as a function of excitation wavelength by using a monochromator with single grating in Czerny-Turner optical design, in AC mode with a chopping frequency of 1 Hz and a bias of blue light (0.3 sun). Absorption spectra of the sensitized photoanodes were recorded on a V-570 Jasco spectrophotomer.

DSSCs have been prepared adapting a procedure reported in the literature [13]. In order to exclude metal contamination all of the containers were in glass or Teflon and were treated with EtOH and 10% HCl prior to use. Plastic spatulas and tweezers have been used throughout the procedure. FTO glass plates were cleaned in a detergent solution for 15 min using an ultrasonic bath, rinsed with pure water and EtOH. After treatment in a UV-O_3 system for 18 min, the FTO plates were treated with a freshly prepared 40 mM aqueous solution of $TiCl_4$ for 30 min at 70 °C and then rinsed with water and EtOH. A transparent layer of 0.20 cm^2 was screen-printed using a 20-nm transparent TiO_2 paste (Solaronix T/SP). The coated transparent film was dried at 125 °C for 6 min and then another layer was screen-printed by using a light scattering TiO_2 paste with particles > 100 nm (Solaronix R-SP). The coated films were thermally treated at 125 °C for 6 min, 325 °C for 10 min, 450 °C for 15 min, and 500 °C for 15 min. The heating ramp rate was 5–10 °C/min. The sintered layer was treated again with 40 mM aqueous $TiCl_4$ (70 °C for 30 min), rinsed with EtOH and heated at 500 °C for 30 min. After cooling down to 80 °C the TiO_2 coated plate was immersed into a proper solution of the dye (see text for details) for 20 h at room temperature in the dark.

Counter electrodes were prepared according to the following procedure: a 1-mm hole was made in a FTO plate, using diamond drill bits. The electrodes were then cleaned with a detergent solution for 15 min using an ultrasonic bath, 10% HCl, and finally acetone for 15 min using an ultrasonic bath. After thermal treatment at 500 °C for 30 min, a 15 μL of a 5×10^{-3} M solution of H_2PtCl_6 in EtOH was added and the thermal treatment at 500 °C for 30 min repeated. The dye adsorbed TiO_2 electrode and Pt-counter electrode were assembled into a sealed sandwich-type cell by heating with a hot-melt ionomer-class resin (Surlyn 30-μm thickness) as a spacer between the electrodes. A drop of the electrolyte solution was added to the hole and introduced inside the cell by vacuum backfilling. Finally, the hole was sealed with a sheet of Surlyn and a cover glass. A reflective foil at the back side of the counter electrode was taped to reflect unabsorbed light back to the photoanode.

3. Results and discussion

3.1. Syntheses

Our synthetic route to the helicene-based dye **1** is shown in Scheme 1. The dialdehyde **2** [5d] was employed as the starting compound. By adjusting the reaction stoichiometry, it was possible to selectively react the two formyl groups with two different reagents in order to obtain the dye **1**.

The triarylamine group was introduced through a Wittig reaction between one formyl group on helicene **2** and phosphonium salt **3** [7]. The slow addition of a solution of **3** in DMF to a suspension of the dialdehyde **2**, K_2CO_3 and a catalytic amount of 18-crown-6 in DMF gave the intermediate **4** in 67% yield. Next, the introduction of the acceptor unit under Knoevenagel condensation conditions provided dye **1** as a dark red solid in 60% yield. Moreover, we reasoned that the introduction of only the acceptor unit in the helicene **6** could give the simplified push-pull system **5**, in which the unsubstituted thiophene ring at one end of the helical scaffold could act as a donor group. We therefore synthesized compound **5** to check its performance as DSSC dye in comparison with dye **1**. The Knoevenagel condensation between the monoaldehyde **6** [5c] and cyanoacetic acid gave the cyanoacrylic acid **5** in 82% yield (Scheme 1).

3.2. UV–vis absorption properties

The absorption spectra of **1**, **5** and the unsubstituted tetrathiahelicene **7** in diluted CH_2Cl_2 solution are shown in Fig. 2, and the photophysical data collected in Table 1.

As expected, due to the more extended π-system, the absorption of **1** and **5** resulted to be red-shifted of 30–40 nm in comparison with the one of the unsubstituted helicene **7**. Dyes **1** and **5** exhibit almost the same absorption peak, with the latter being slightly red-shifted compared to

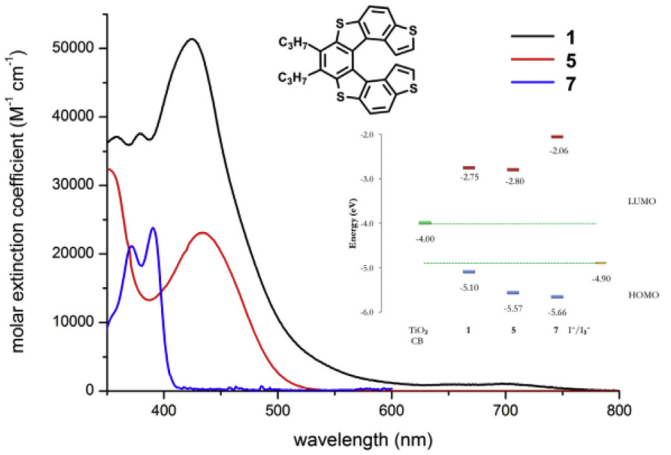

Fig. 2. UV–vis absorption spectra and HOMO-LUMO values of compounds **1**, **5** and **7**.

the former. The effect of the donor triarylamino unit is mostly in terms of molar extinction coefficient in **1**, which is more than twice than that in **5**. This effect has been detailed in terms of oscillator strength (f) and transition dipole moment ($\mu_{(GE)}$) (Table 1).

Indeed, the oscillator strength (f) of **1** is twice higher than that of **5** and five times higher than that of the unsubstituted system **7**. The experimental value of the oscillator strength is in very good agreement with the computed value (*vide infra*). It is therefore evident that the compound **1** owns the better optical properties in terms of light harvesting. The presence of the donor triarylamino unit enhances the ground to excited state transition (associated to the intramolecular charge transfer, ICT), as evidenced by the much higher transition dipole moment.

3.3. Electrochemical properties

The electron transfer properties of chromophores **1** and **5** have been studied by cyclic voltammetry (CV), and have been conveniently discussed comparing the CV features of tetrathiahelicene **7** [14] (Table 1, and Figs. 1–2 in Ref. [15]). Concerning dye **5**, the addition of a single cyanoacrylic group to the helical backbone provided on the cathodic side a new, more favorable, reduction site (at −2.00 V respect to −2.74 V *vs* $Fc^+|Fc$ for **7**, Figs. 1–2 in Ref. [15]). Moreover, it apparently results in differentiation between the oxidation potentials, one resembling the 7-TH scaffold (0.77 V and 0.86 V *vs* $Fc^+|Fc$, respectively, Fig. 2 in Ref. [15]), and the following possibly corresponding to the electron-poorer moiety, shifted to a much higher potential (0.98 V *vs* $Fc^+|Fc$).

In the CV patterns of **1**, the first oxidation peak, chemically and electrochemically reversible, should be attributed to the bis(para-methoxyphenyl)phenylamine [16] conjugated to the linker (it is observed at nearly the same potential in the new chromophore, 0.30 V and 0.34 V *vs* $Fc^+|Fc$, respectively, Figs. 1–2 in Ref. [15]). The first chemically and electrochemically reversible reduction peak can be attributed to the cyanoacrylic group conjugated to the linker. The less extreme oxidation and reduction potentials, and narrower HL gap of **1**, are consistent with the higher effective conjugation of the more extended helicene system, only partially attenuated by the torsional angle.

Table 2
Excitation energies, oscillator strengths and characterization/localization of the six energetically lowest electronically excited singlet states calculated at the TD-DFT/ωB97XD/cc-pVDZ level of theory.

Excited state	Excitation energy [eV]	Oscillator strength	Character/ localization
S_1	2.8458	0.1862	CT D– > A
S_2	3.3154	0.2087	local TTH/A
S_3	3.4822	1.2911	local TTH/D
S_4	3.5774	0.1997	local/CT TTH– > A
S_5	3.9233	0.1489	local TTH/A
S_6	4.0051	0.1883	CT/local TTH– > A

Abbreviations for the characterization/localization: TTH = tetrathiahelicene, D = donor subsystem, A = acceptor subsystem, CT = charge transfer.

3.4. Theoretical calculations

We have also carried out DFT [17] calculations to further probe the structural features and the charge excitation behaviour of **1**. After optimization of the initial ground state structure of **1**, the first six electronically excited singlet states have been calculated at the TD-DFT/ωB97XD/cc-pVDZ level of theory [8,9,18]. The excitation energies, oscillator strengths and both the character and the localization of the calculated excited states are given in Table 2.

Using the molecular orbital (MO) picture, the excitations cannot clearly be characterized and localized due to a multitude of contributing orbital transitions. Thus, for a detailed analysis of the electronically excited states, the transition density matrix was analysed and natural transition orbitals (NTOs) [19] have been calculated (see Table 1 in Ref. [15]). In contrast to normal MOs, these orbitals describe directly the electronical excitation and are thus specific for each excited state. Using the NTOs, the character and the localization of the electron transition can be directly visualized.

As can be seen, the first excited state is clearly a charge-transfer state from the donating moiety to the acceptor. It shows a rather small oscillator strength of 0.19. However, the 7-TH linker as a separator still contributes largely to the total excitation since the π-system is delocalized over all three subgroups. In contrast, the S_3 state exhibits an oscillator strength of 1.29, and therefore is referred to as the bright state. It is characterized by mainly a $\pi \rightarrow \pi^*$ transition localized on the 7-TH moiety and the donor subsystem. Similar to this bright state is the S_2

Table 1
Optical and electrochemical characterization of dyes **1** and **5**, in comparison with tetrathiahelicene **7**.

Optical data					Electrochemical data				
compd	λ_{max}[a] (nm)	ε ($M^{-1}cm^{-1}$)	f	$\mu_{(GE)}$ (D)	$E_{p\,c}$ *vs* $Fc^+|Fc$ (V)	LUMO (eV)[b]	$E_{p\,a}$ *vs* $Fc^+|Fc$ (V)	HOMO (eV)[b]	HL gap (eV)
1	424	51400 ± 100	1.41	11.3	−2.39	−2.75	0.30	−5.10	2.35
					−2.22		0.45		
					−2.05		1.03		
5	434	23100 ± 100	0.68	7.8	−2.23	−2.80	0.77	−5.57	2.77
					−2.00		0.98		
							1.09		
7	390	23800 ± 100	0.28	4.9	−2.74	−2.06	0.86	−5.66	3.60

[a] Concentration: 10^{-5} M in DCM.
[b] The values are calculated as: HOMO (LUMO) = − *e* [E_p, I_a *vs* $Fc^+|Fc$ (E_p, I_c *vs* $Fc^+|Fc$) + 4.8].

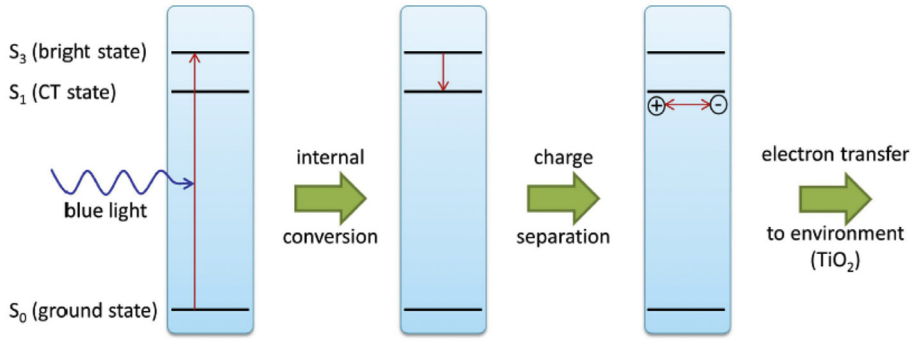

Fig. 3. Scheme of the charge separation process after photoexcitation.

state, which shows a local π → π* transition but with contributions on the acceptor group. The energetically higher lying states S_4, S_5 and S_6 show a mixture of local and charge-transfer character mainly localized on the 7-TH and the acceptor moiety.

From these calculations, the following picture can be drawn: absorption of blue light will most probably lead to an excitation and population of the bright state (S_3). Via internal conversion, the first excited state gets populated. This state is a charge-transfer state, and thus leads to a charge separation. The separated charges can in the following process be transferred to the TiO_2 surface and used as electric energy. This process is illustrated in the scheme in Fig. 3.

3.5. Photovoltaic performance

In order to test the potential of synthesized helicene-based dyes, the PV performances of liquid DSSCs sensitized by **1** and **5** were investigated (Table 3). The devices were prepared using a double-layer film of TiO_2 (10 μm transparent + 5 μm scattering layer). The devices were tested with and without 3a, 7a-dihydroxy-5b-cholic acid (CDCA) as a co-adsorbent agent to prevent detrimental aggregation [20]. The overall power conversion efficiencies (PCE) were derived from PCE = J_{sc} x V_{oc} x FF, where J_{sc} is the short circuit current density, V_{oc} the open circuit voltage, and FF the fill factor. Fig. 4A shows the current/voltage curves of cells with CDCA and the ones without are reported in Fig. 3 in Ref. [15].

Data clearly show that the PV efficiency in presence of CDCA are higher than those obtained without the co-adsorbent. Considering the best performing cells, the efficiency of those prepared with the donor-acceptor dye **1-CDCA** is higher than that of **5-CDCA**, bearing only the acceptor unit. The performances of the devices without CDCA follow the same trend previously described but expressing a slightly lower photovoltages even with similar photocurrents. The higher current is in agreement with the better experimental and computed optical properties, suggesting that the presence of the donor-acceptor architecture promotes ICT and subsequent electron injection to TiO_2. The highest PCE efficiency, recorded for **1-CDCA** at 0.5 sun, is higher than 2%, which is noteworthy taking into account the helical geometry of the spacer.

To gain further insights, incident monochromatic photon-to-current conversion efficiencies (IPCE) were investigated (Fig. 4B). The photocurrent values calculated by IPCE nicely matched the experimental values (masked cells). The shape resembles the corresponding absorption spectra. The IPCE peaks are around 50%. In particular, the IPCE of **1-CDCA** is significantly red-shifted compared to **5-CDCA**, with a value > 40% over a broad range. To better elucidate the different contributions, the two components of the IPCE according to equation IPCE(λ) = LHE(λ) x APCE (λ), where LHE is the light-harvesting efficiency and APCE the absorbed monochromatic photon-to-current conversion efficiency, were investigated (Fig. 4C–D). The best LHE profile is associated to the donor-acceptor dye **1-CDCA**, thus confirming that the higher current originates from the stronger light harvesting ability. The internal quantum efficiency APCE was very high for both dyes, with values of 90–100% over a broad range.

Table 3
PV characteristics of DSSC sensitized by dyes **5** and **1** with and without CDCA at different light intensities (AM 1.5 standard conditions).[a,b]

Dye	Irradiance	J_{sc}		V_{oc}		FF		PCE	
	[sun]	[mA cm^{-2}]		[mV]		[%]		[%]	
1[c]	1.0	4.3	(5.3)	608	(617)	73	(71)	1.9	(2.3)
	0.5	2.4	(2.9)	585	(596)	73	(71)	2.0	(2.2)
1-CDCA[c]	1.0	4.6	(5.1)	660	(670)	75	(76)	2.3	(2.6)
	0.5	2.4	(2.8)	637	(650)	76	(76)	2.3	(2.7)
5[c]	1.0	2.4	(3.3)	551	(561)	73	(72)	1.0	(1.4)
	0.5	1.2	(1.8)	530	(544)	73	(72)	1.0	(1.4)
5-CDCA[c]	1.0	3.1	(3.6)	637	(633)	80	(75)	1.5	(1.7)
	0.5	1.6	(1.9)	603	(615)	78	(78)	1.5	(1.8)
N719[d]	1.0	15.6	(17.9)	720	(720)	72	(71)	8.1	(9.2)

[a] CDCA:dye ratio 0:1 and 1:1.
[b] Values without a black shading mask on top of the cell are listed in brackets.
[c] Dye solution 2×10^{-4} M in EtOH (15 mL EtOH), electrolyte Z960 (1.0 M N,*N*-dimethylimidazolium iodide. 0.03 M I_2, 0.05 M LiI, 0.1 M guanidinium thiocyanate, and 0.5 M 4-*t*-butylpyridine in acetonitrile/valeronitrile 85/15).
[d] Dye solution of 5×10^{-4} M in EtOH solution; electrolyte A6141 (0.6 M N-butyl-*N*-methylimidazolium iodide, 0.03 M I_2, 0.1 M guanidinium thiocyanate, and 0.5 M 4-*t*-butylpyridine in acetonitrile/valeronitrile 85:15).

4. Conclusions

In summary, we have described the first example of a push-pull dye, in which an unconventional nonplanar tetrathiahelicene scaffold was used as the π-spacer between the two donor and acceptor groups. The presence of the contorted polyheteroaromatic π-spacer, and the mutual location of acceptor and donor groups do not hamper a complete conjugation of the molecule, which exhibit suitable HOMO–LUMO levels to be used in DSSC. The presence of the donor-acceptor architecture is necessary to observe very good performances in DSSC. In fact, higher internal charge transfer, and subsequent electron injection to the conduction band of TiO_2 was detected for compound **1** compared to compound **5**, while lower experimental and computed optical properties, lower oscillator strength and transition dipole moment as well as lower photocurrent were observed for compound **5**.

Acknowledgments

D. D. and S. C. thank the Università degli Studi di Milano for the PhD and post-doctoral fellowship, respectively.

This research did not receive any specific grant from funding agencies in the public, commercial, or not-for-profit sectors.

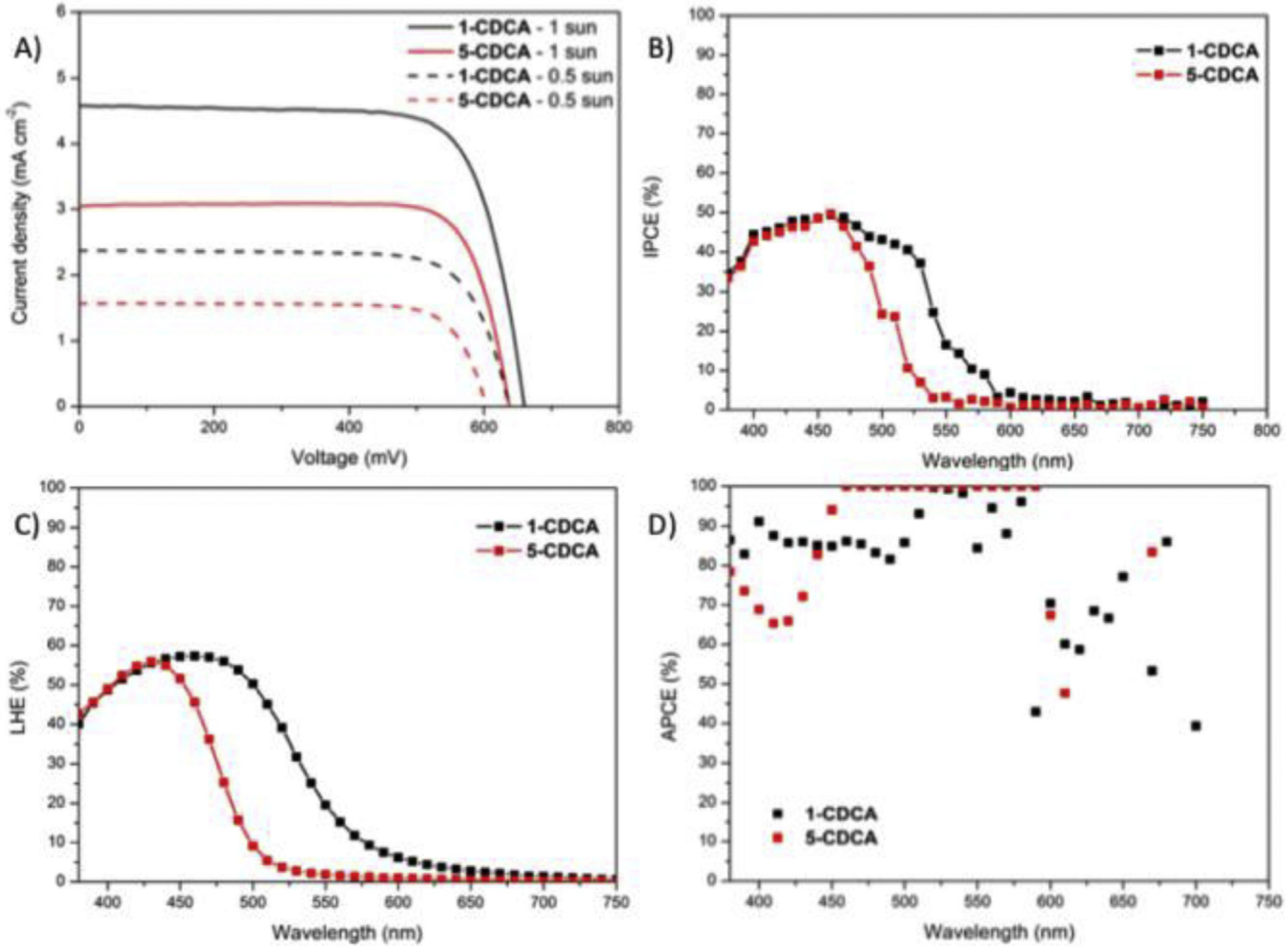

Fig. 4. (A) *J/V* curves of DSSC sensitized by **1-CDCA** and **5-CDCA**, with different solar intensities. (B) Corresponding IPCE plots. (C) Corresponding LHE lots obtained using a 5-μm transparent TiO_2 film. (D) Corresponding APCE plots.

References

[1] (a) Collins SK, Vachon MP. Unlocking the potential of thiaheterohelicenes: chemical synthesis as the key. Org Biomol Chem 2006;4:2518–24https://doi.org/10.1039/B603305A;
(b) Shen Y, Chen CF. Helicenes: synthesis and applications. Chem Rev 2012;112:1463–535. https://doi.org/10.1021/cr200087r;
(c) Licandro E, Cauteruccio S, Dova D. Thiahelicenes: from basic knowledge to applications. Adv Heterocycl Chem 2016;118:1–46https://doi.org/10.1016/bs.aihch.2015.12.001;
(d) Chen CF, Shen F. Helicene chemistry, from synthesis to application. Berlin Heidelberg: Springer-Verlag; 2017. https://doi.org/10.1007/978-3-662-53168-6.

[2] (a) Kim C, Marks TJ, Facchetti A, Schiavo M, Bossi A, Maiorana S, et al. Synthesis, characterization, and transistor response of tetrathia[7]helicene precursors and derivatives. Org Electron 2009;10:1511–20https://doi.org/10.1016/j.orgel.2009.08.018;
(b) Bossi A, Licandro E, Maiorana S, Rigamonti C, Righetto S, Stephenson GR, et al. Theoretical and experimental investigation of electric field induced second harmonic generation in tetrathia[7]helicenes. J Phys Chem C 2008;112:7900–7. https://doi.org/10.1021/jp7117554.

[3] (a) Cauteruccio S, Bartoli C, Carrara C, Dova D, Errico C, Ciampi G, et al. A nanostructured PLGA system for cell delivery of a tetrathiahelicene as a model for helical DNA intercalators. Chem Plus Chem 2014;80:490–3https://doi.org/10.1002/cplu.201402347;
(b) Shinohara K, Sannohe Y, Kaieda S, Tanaka K, Osuga H, Tahara H, et al. A chiral wedge molecule inhibits telomerase activity. J Am Chem Soc 2010;132:3778–82. https://doi.org/10.1021/ja908897j;
(c) Xu Y, Zhang YX, Sugiyama H, Umano T, Osuga H, Tanaka K. (P)-Helicene displays chiral selection in binding to Z-DNA. J Am Chem Soc 2004;126:6566–7. https://doi.org/10.1021/ja0499748.

[4] (a) Dova D, Viglianti L, Mussini PR, Prager S, Dreuw A, Voituriez A, et al. Tetrathia[7]helicene phosphorus derivatives: experimental and theoretical investigations of electronic properties, and preliminary applications as organocatalysts. Asian J Org Chem 2016;5:537–49https://doi.org/10.1002/ajoc.201600025;
(b) Cauteruccio S, Dova D, Benaglia M, Genoni A, Orlandi M, Licandro E. Synthesis, characterisation, and organocatalytic activity of chiral tetrathiahelicene diphosphine oxides. Eur J Org Chem 2014:2694–702https://doi.org/10.1002/ejoc.201301912;
(c) Cauteruccio S, Loos A, Bossi A, Blanco Jaimes MC, Dova D, Rominger F, et al. Gold(I) complexes of tetrathiaheterohelicene phosphanes. Inorg Chem 2013;52:7995–80044. https://doi.org/10.1021/ic4005533;
(d) Monteforte M, Cauteruccio S, Maiorana S, Benincori T, Forni A, Raimondi L, et al. Tetrathiaheterohelicene phosphanes as helical-shaped chiral ligands for catalysis. Eur J Org Chem 2011:5649–58https://doi.org/10.1002/ejoc.201100726.

[5] (a) Waghray D, de Vet C, Karypidou K, Dehaen W. Oxidative transformation to naphthodithiophene and thia[7]helicenes by intramolecular Scholl reaction of substituted 1,2-bis(2-thienyl)benzene precursors. J Org Chem 2013;78:11147–54. https://doi.org/10.1021/jo401807x;
(b) Waghray D, Dehaen W. A fragment based approach toward thia[*n*]helicenes. Org Lett 2013;15:2910–3. https://doi.org/10.1021/ol400825w;
(c) Waghray D, Nulens W, Dehaen W. Efficient synthesis of benzo fused tetrathia[7]helicenes. Org Lett 2011;13:5516–9. https://doi.org/10.1021/ol202236r;
(d) Licandro E, Rigamonti C, Ticozzelli MT, Monteforte M, Baldoli C, Giannini C, et al. Synthesis and functionalization of novel tetrathia[7]helicenes as new push-pull systems. Synthesis 2006:3670–8. https://doi.org/10.1055/s-2006-950222.

[6] Dova D, Cauteruccio S, Prager S, Dreuw A, Graiff C, Licandro E. Chiral thiahelicene-based alkyl phosphine-borane complexes: synthesis, X-ray characterization, and theoretical and experimental investigations of optical properties. J Org Chem 2015;80:3921–8. https://doi.org/10.1021/acs.joc.5b00243.

[7] Dalton LR, Jen AKY, Londergan T, Carlson WB, Phelan G, Huang D et al WO/2002/008215, PCT/US2001/023339, 2002.

[8] Chai JD, Head-Gordon M. Long-range corrected hybrid density functionals with damped atom-atom dispersion corrections. Phys Chem Chem Phys 2008;10:6615–20https://doi.org/10.1039/B810189B.

[9] Dunning TH. Gaussian basis sets for use in correlated molecular calculations. I. The atoms boron through neon and hydrogen. J Chem Phys 1989;90:1007–23https://doi.org/10.1063/1.456153.

[10] Frisch MJ, Trucks GW, Schlegel HB, Scuseria GE, Robb MA, Cheeseman JR, et al. Gaussian 09; Revision D.01. Wallingford CT: Gaussian, Inc.; 2013.
[11] Hanwell MD, Curtis DE, Lonie DC, Vandermeersch T, Zurek E, Hutchison GR. Avogadro: an advanced semantic chemical editor, visualization, and analysis platform. J Cheminf 2012;4:17https://doi.org/10.1186/1758-2946-4-17.
[12] Persistence of Vision Raytracer Pty. Ltd: POV-Ray 3.7. http://www.povray.org.
[13] Ito S, Murakami TN, Comte P, Liska P, Grätzel C, Nazeeruddin MK, et al. Fabrication of thin film dye sensitized solar cells with solar to electric power conversion efficiency over 10%. Thin Solid Films 2008;516:4613–9https://doi.org/10.1016/j.tsf.2007.05.090.
[14] Bossi A, Falciola L, Graiff C, Maiorana S, Rigamonti C, Tiripicchio A, et al. Electrochemical activity of thiahelicenes: structure effects and electrooligomerization ability. Electrochim Acta 2009;54:5083–97https://doi.org/10.1016/j.electacta.2009.02.026.
[15] Dova D, Cauteruccio S, Manfredi N, Prager S, Dreuw A, Arnaboldi S, et al. An unconventional helical push-pull system for solar cells. Data in Brief 2018. [submitted] for publication.
[16] Longhi E, Bossi A, Di Carlo G, Maiorana S, De Angelis F, Salvatori P, et al. Metal-free benzodithiophene-containing organic dyes for dye-sensitized solar cells. Eur J Org Chem 2013:84–94https://doi.org/10.1002/ejoc.201200958.
[17] (a) Kohn W, Sham LJ. Self-consistent equations including exchange and correlation effects. Phys Rev 1965;140:A1133–8https://doi.org/10.1103/PhysRev.140.A1133;
(b) Hohenberg P, Kohn W. Inhomogeneous electron gas. Phys Rev 1964;136:B864–71https://doi.org/10.1103/PhysRev.136.B864.
[18] Dreuw A, Head-Gordon M. Single-reference ab initio methods for the calculation of excited states of large molecules. Chem Rev 2005;105:4009–37. https://doi.org/10.1021/cr0505627.
[19] (a) Martin RL. Natural transition orbitals. J Chem Phys 2003;118:4775–7https://doi.org/10.1063/1.1558471;
(b) Luzanov AV, Sukhorukov AA, Umanskii VE. Application of transition density matrix for analysis of excited states. Theor Exp Chem 1976;10:354–61https://doi.org/10.1007/BF00526670.
[20] Lee KM, Chen CY, Wu SJ, Chen SC, Wu CG. Surface passivation:the effect of CDCA co-adsorbent and dye bath solvent on the durability of dye-sensitized solar cells. Sol Mater Sol Cells 2013;108:70–7https://doi.org/10.1016/j.solmat.2012.08.008.